



# Modeling dynamic stall of a straight blade vertical axis wind turbine



K.M. Almohammadi<sup>a,b,\*</sup>, D.B. Ingham<sup>b</sup>, L. Ma<sup>b</sup>, M. Pourkashanian<sup>b</sup>

<sup>a</sup> Mechanical Engineering Department, Tiabah University, Saudi Arabia

<sup>b</sup> Centre for Computational Fluid Dynamics, Energy Technology and Innovation Initiative (ETTI), University of Leeds, Leeds LS2 9JT, UK

## ARTICLE INFO

### Article history:

Received 25 March 2014

Accepted 6 June 2015

### Keywords:

Straight blade vertical axis wind turbine (SB-VAWT)

Dynamic stall

Laminar separation bubble

Computational fluid dynamics

Transitional modeling

## ABSTRACT

This paper investigates the development of the dynamic stall of a full straight blade vertical axis wind turbine (SB-VAWT) using computational fluid dynamic modeling for solving the 2D Navier–Stokes equations. The 2D unsteady Navier–Stokes equations are solved with the concept of Reynolds averaging. A mesh independency test is analyzed using the General Richardson Extrapolation technique. Two turbulence models are applied, namely the SST  $k-\omega$  and the Transition SST models. It has been found that the stall development is extremely sensitive to the transitional modeling and small laminar separation bubbles will only be accurately predicted by accounting for the transition. However, the transition affects the overall turbine performance by up to 20% and delays the peak of the predicted torque by about 11°, and therefore it is crucial to include laminar-turbulence transition in the design and optimization process of SB-VAWTs.

© 2015 Elsevier Ltd. All rights reserved.

## 1. Introduction

New resources of energy, one of which is wind energy, have been under researchers focus for the last few decades due to the increasing consumption of energy. The interest in the vertical axis wind turbines (VAWTs) has been growing due to its aerodynamic advantages in urban regions where wind may be harvested more efficiently compared to the horizontal axis wind turbines (HAWTs) (Paraschivoiu, 2002; Sharpe, 1977; Wang et al., 2010a). The wind flow structure in urban regions is a research field on its own due to its complexity caused by the high surface roughness values (Balduzzi et al., 2012). Because of this, a uniform flow approaching a turbine is required to be analyzed for the flow structure developed by the turbine and this is complex. It should be noted that the wind speed in urban regions is usually low and this makes the turbine power coefficient peak at low tip speed ratios (typically  $TSR \leq 1-3$ ), which is the ratio of the rotational speed of the turbine blade to the undisturbed wind speed.

A comprehensive understanding of the flow structure of VAWTs under low TSRs is extremely important and this is mainly because of the presence of the unsteady phenomenon of dynamic stall which is a result of unsteady separation and the reattachment, separation bubbles and the vortex shedding into the wake. In the dynamic stall process, the lift overshoots and the performance enhances for a short period of time. This is followed by a sharp drop in the lift and as a result the turbine performance drops. After that, the boundary layer will be in a recovery process. In this context, the dynamic stall is seen to limit the turbine overall performance. This phenomenon mainly limit the VAWT performance and

\* Corresponding author. Tel.: +44 113 3435113; fax: +44 113 246 7310.

E-mail addresses: [ml07kma@leeds.ac.uk](mailto:ml07kma@leeds.ac.uk), [Doctorkmsa@gmail.com](mailto:Doctorkmsa@gmail.com) (K.M. Almohammadi).

Nomenclature			
<i>Symbols</i>		$\alpha$	angle of attack, deg
$C$	chord length, m	$\Gamma$	diffusion coefficient, m <sup>2</sup> /s
$c_p$	power coefficient $\left[ \frac{\text{Power}}{0.5\rho AV^3} \right]$	$\lambda$	tip speed ratio (TSR)
$d$	turbine diameter, m	$\rho$	air density, kg/m <sup>3</sup>
$E$	turbulence destruction sources	$\theta$	azimuthal angle, deg
$p^*$	order of accuracy	$k$	kinetic energy, m <sup>2</sup> /s <sup>2</sup>
$P$	turbulence transition sources	$\varepsilon$	turbulence dissipation, m <sup>2</sup> /s <sup>2</sup>
$R$	refinement ratio	$\omega$	specific dissipation rate, m <sup>2</sup> /s <sup>3</sup>
$\bar{R}$	convergence condition	<i>Subscripts</i>	
$\bar{Re}_{ot}$	momentum thickness, m	$\varepsilon$	turbulence dissipation
$t$	time, s	$ij$	direction tensors
$\omega$	rotational speed, rad/s	$k$	kinetic energy
$U, U_\infty$	undisturbed flow, m/s	$\omega$	specific dissipation rate
<i>Greek symbols</i>		$\gamma$	intermittency

make their modeling a challenging task where the computational error could be increased from the modeling of the physics of the problem by selecting an inappropriate turbulence model, or from the numerical simulations by employing insufficient computational points in the regions of complex air flow. At low TSRs, the dynamic stall becomes severe and this makes predicting the torque experimentally a relatively challenging task and therefore only a few experiments may be found in the literature (Wang et al., 2010a). In the selected experiment, where the required conditions for investigating the dynamic stall are present, only the power produced by the turbine was measured and unfortunately there is no instantaneous torque measurement.

The straight blade VAWT is of the family of the Darrieus turbines which operate on the principle of the lift force. Despite this its geometry is relatively simple, and it develops complex flow aerodynamics, such as dynamic stall and vortex shedding into the wake.

Dynamic stall is an unsteady nonlinear phenomenon which is mainly caused by the change in the angle of attack (AOA) of the airfoils of the turbine and the aerodynamic forces are significantly affected by the presence of the dynamic stall. In VAWTs, the angle of attack changes rapidly during operation and this makes the dynamic stall more severe. At low tip speed ratios, the angle of attack could be as high as approximately  $\pm 90^\circ$  (Ferreira et al., 2007; Islam et al., 2009). The dynamic stall occurrence causes a loss in the lift force due to the flow separation from the airfoil surface and this could result in a relatively higher lift loss for a full cycle of AOA compared to the static stall (Ham, 1968; Jones, 1933; McCroskey et al., 1975b; Wang et al., 2012). This is because the reattachment of the flow may not occur until the angle of attack of the airfoil is much lower than the static stall angle (Tsang et al., 2008). The process of separation and reattachment strongly affects the unsteady aerodynamics of the airfoil (Leishman, 2006). The leading edge vortex development and shedding is the main reason for the dynamic stall. The vortex moves backwards to the trailing edge over the airfoil surface and this creates additional vortices. When the vortex is shed into the wake from the airfoil surface, the airfoil experiences a sudden loss of lift and moment and this has been explained by Ham (1968).

One of the first investigations of the dynamic stall phenomenon was performed by Kramer in 1932 (Leishman, 2006). He observed that the flow over a lifting airfoil remains attached beyond the static angle of attack. Because of the complexity of the dynamic stall, empirical investigations have not been possible, and therefore researchers have combined experimental inputs into their analysis. In 1981, McCroskey concluded that the theoretical methods available for analyzing dynamic stall need significant improvement. In 1990, Leishman reported that a thorough theoretical study of the dynamic stall can only be obtained using the full Navier–Stokes equations, which is the basis of this investigation, with a suitable turbulence model (Leishman, 1990). Over the last few years, performing simulations on the Navier–Stokes equations has become feasible due to the significant improvement in the available computational power. Many attempts have been devoted to the understanding of dynamic stall experimentally (Carr, 1988; Carta, 1979; Ericsson and Reding, 1983; Favier et al., 1988; McAlister, 1982; McCroskey et al., 1975a, 1982). However, even though the stages of the dynamic stall have each been well investigated, the dynamic stall as a phenomenon requires a more in depth investigation (Mulleners and Raffel, 2011). Many attempts using computational fluid dynamics (CFD) techniques for oscillating airfoils may be found in the literature with the aim of analyzing the air flow in the vicinity of the airfoil developing dynamic stall (Gharali and Johnson, 2012; Wang et al., 2010a, 2012, 2010b). Due to the high sensitivity of the stall phenomenon, it is important to investigate the air flow on three airfoils of VAWTs in addition to analyzing a single airfoil in order to account for the air flow interaction in the vicinity of the airfoils and in the wake which may affect the development of the stall. The techniques of analyzing the air flow in VAWTs that are widely applied are essentially based on the stream tube theory (Paraschivoiu, 1988; Paraschivoiu and Delclaux, 1983), vortex

theory (Cardona, 1984; Strickland et al., 1980), and cascade theory (Islam et al., 2008). These models need to be modified for the viscous sub layer calculations in order to account for the dynamic stall. Therefore, the full Navier–Stokes equations should be employed. However, the analysis of the VAWTs found in the literature focuses on the turbine loading and performance compared to the experimental investigations (Gupta and Biswas, 2010; Hwang et al., 2009; Kooiman and Tullis, 2010; McLaren, 2011). The analysis of the dynamic stall developed by VAWTs has to be performed on a system of three airfoils rotating rather than one airfoil oscillating or rotating.

This paper focuses on investigating the development of the dynamic stall on straight blade vertical axis wind turbines (SB-VAWTs) using the 2D incompressible Navier–Stokes equations with two turbulence models, namely the SST  $k-\omega$  and the Transition SST (SST Transitional) models. The predicted power coefficient is compared against the power coefficient measured in the experiment (Bravo et al., 2007; Kooiman and Tullis, 2010). However, the mesh independent solution for the computations performed is estimated by employing the General Richardson method in order to compare the mesh independent solution produced, regardless of the experimental data, to the solution obtained using the finest mesh.

## 2. Dynamic stall modeling of vertical axis wind turbines

The flow regime in the vicinity of the straight blades of the vertical axis wind turbines is usually complex at low tip speed ratios. This flow complexity is mainly caused by the continuous change in the blade azimuthal angle, direction and magnitude of the velocity during the turbine operation, and as a result the angle of attack also changes continually. It is important to note that the flow velocity in the region enclosed by the traveling path of the airfoils of the turbine is not constant. Therefore the variation of the angle of attack, namely the local angle of attack ( $\alpha$ ), is given by

$$\alpha = \tan^{-1} \left( \frac{\sin \theta}{\frac{\omega r}{U} + \cos \theta} \right) \quad (1)$$

where  $\theta$ ,  $U$ ,  $\omega$ ,  $r$  are the azimuthal angle of the airfoil, undisturbed flow, airfoil rotational speed and turbine radius, respectively. The variation of the angle of attack given by Eq. (1) in the upstream region of the turbine is different when compared to the downstream side which adds further complexity to the dynamic stall analysis. The schematic of the air flow crossing the turbine and the typical peaks and troughs of the power coefficient at TSR 1.75 is shown in Fig. 1. The change in the local angle of attack is an important parameter in the development of the dynamic stall which inherently affects the turbine operation at low tip speed ratios ( $TSR < 5$ ) (Ferreira et al., 2009). When the local angle of attack of the VAWT airfoil exceeds the static stall angle, the airfoil is under dynamic stall conditions, and as a result the loss of lift is delayed due to the formation of the leading edge vortex. This vortex moves down the airfoil surface and causes an increase in the lift and as the flow separates from the airfoil surface a sudden and sharp drop in the lift affects the overall performance of the turbine. However, this process is often explained by investigating oscillating airfoils but to fully understand the development of the dynamic stall on the VAWT then the full rotating model must be investigated. This is mainly due to the high sensitivity of the dynamic stall to the flow conditions, such as the Reynolds number and the turbine reduced frequency which are well explained in Richter et al. (2011).

The attempts to analyze dynamic stall that is developed in VAWTs have been mainly based on the experimental data and this is due to the mathematical modeling difficulties (Fraunie et al., 1986; Laneville and Vittecoq, 1986). In recent years, the advancement of experimental equipment has allowed flow field measurements of the VAWTs to be made using such techniques as particle image velocimeter (PIV) techniques (Ferreira et al., 2009; Fujisawa and Shibuya, 2001).

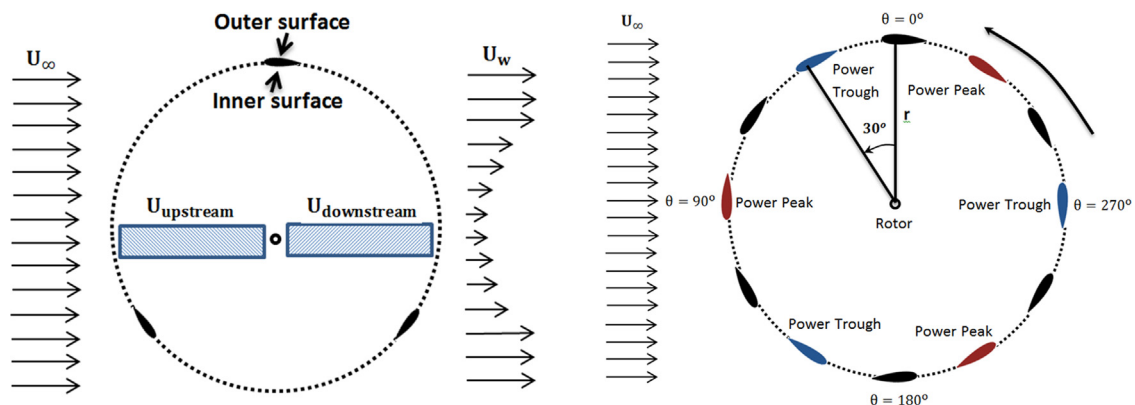


Fig. 1. Schematic of the SB-VAWT.

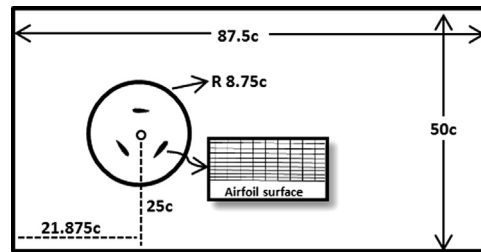


Fig. 2. 2D computational domain for the wind turbine.

### 3. Computational scheme

#### 3.1. Computational domain and grid

The turbine geometry investigated in this paper consists of three NACA0015 straight blades with a chord length of 0.4 m where the trailing edge of the blade is curved by 10% of the chord length ( $0.1c$ ). The turbine radius is  $3.125c$  and the blade height is  $7.5c$ . The computational domain is created as a 2D model based on the experimental setup of Bravo et al. (2007) and Kooiman and Tullis (2010). The solution domain, as shown in Fig. 2, (Castelli et al., 2011) consists of a rotating and a stationary region where the stationary region is created as a rectangle which is  $87.5c$  in length and  $50c$  in width, and the rotating region is created as a circle of radius  $8.75c$ . These dimensions are based on the domain size independency analysis performed by McLaren (2011) and it is fixed for all the computations presented in this paper in order to reproduce the results obtained experimentally.

The boundary conditions are set to be the same as in the experimental investigation in order to compare the predicted power coefficient to the experimental results. The left hand side of the rectangle is set as inlet boundary conditions whereas the other three sides are set as pressure outlet boundaries with zero gauge pressure (1 atm) because the experiment is performed on top of a building. An interface boundary condition is set between the rotating and stationary domain in order to apply the sliding mesh technique to employ the turbine rotation.

There are two types of cells that are commonly used in 2D numerical computations, namely quadrilateral and triangular cells. It is desirable to create a quadrilateral based mesh because of the complexity of the air flow. This is mainly due to the convergence stability, producing relatively lower numerical diffusion compared to using triangular cells, and the solution consistency associated with grid refinement that is usually experienced when applying quadrilateral cells (Tu et al., 2008; Versteeg and Malalasekera, 2007). Therefore, structured high quality quadrilateral cells, with a  $y^+$  (the relative distance of the first node from the surface of the airfoil) value of about 1 are generated in the airfoil boundary layer which is estimated to be of thickness  $0.75$  mm (Acheson, 1990) by employing the relation  $(\delta/c) \sim Re^{-1/2}$ , based on the airfoil chord length (0.4 m) and the flow Reynolds number ( $Re_c = \rho c U_\infty / \mu = 2.83 \times 10^5$ ) at an upwind speed 10 m/s (inlet velocity). 1888 nodes are equally distributed on each airfoil surface and in the mesh sensitivity analysis the number of nodes are increased to 5000 points in order to understand the dynamic stall development. Since the air speed near the airfoils is relatively higher than the upwind speed, the estimated thickness of the boundary layer based on the upwind speed, namely,  $0.75$  mm is considered to be a conservative value and the actual boundary layer thickness will be contained by the structured mesh. In order to avoid sudden changes in mesh topology, a gradual fixed rate growth of 1.08% has been applied from the airfoil surfaces and this maintains a smooth transport of computational variables across the computational domain. Unstructured quadrilateral cells are generated elsewhere due to difficulties in creating a structured mesh for the rotating airfoils. This results in a grid size of about 135 000–500 000 cells.

#### 3.2. Turbulence model and simulation

One of the most widely used concepts in the analysis of turbulence flows is to apply the averaging concept of the transport quantities in the Navier–Stokes equations and this was originally proposed by Osborne Reynolds in the second half of the 19th century (Eckhardt et al., 2007; Jackson and Launder, 2007; Reynolds, 1895). This concept became the basis for many turbulence models, among which one and two equation models are commonly used. The computational effort and the solution accuracy of these two turbulence models are not similar, and therefore the choice of the turbulence model is important in the modeling process. Understanding the physics of the problem is crucial in selecting the appropriate turbulence model for the problem under investigation. In the case of SB-VAWTs, the region near the airfoils develops complex flow regimes, such as flow separation, flow reattachment, laminar-turbulent transition of the flow, etc. Therefore the selected turbulence model has to account for all these conditions.

In the literature, it has been found that the standard  $k-\omega$  model produces unrealistic results when the case involves flow separation (Baldwin and Lomax, 1978), flow reattachment (Kato and Launder, 1993), flow recovery (Ince and Launder, 1995), unconfined flows (Apsley et al., 1997), and secondary flows (Tu et al., 2008) and all these phenomenon occur in SB-VAWT. The main reason for this failure is due to the assumption related to the turbulence dissipation ( $\epsilon$ ) near the walls. Therefore,

the turbulence dissipation ( $\varepsilon$ ) has been modified to the specific turbulence dissipation rate ( $\omega$ ) and this resulted in  $k$ - $\omega$  turbulence models. A significant improvement of the near wall treatment and separated flow predictions by this model has been reported (Menter et al., 2003). It is important to note that these models assume that the flow is fully developed, which if applied to SB-VAWT, the laminar-to-turbulent transition near the airfoil surface will be suppressed. Recently, Menter and Langtry (Langtry et al., 2006; Menter, 2009; Menter et al., 2006) have incorporated two additional transport variables that account for laminar-to-turbulent transition, namely the intermittency and the momentum thickness which determines the onset of transition. The governing equations are given by

$$\frac{\partial(\rho k)}{\partial t} + \frac{\partial(\rho U_i k)}{\partial x_i} = \widetilde{P}_k - E_k + \frac{\partial}{\partial x_j} \left[ \Gamma_k \frac{\partial k}{\partial x_j} \right] \quad (2)$$

$$\frac{\partial(\rho \omega)}{\partial t} + \frac{\partial(\rho U_i \omega)}{\partial x_i} = P_\omega - E_\omega + D_\omega + \frac{\partial}{\partial x_j} \left[ \Gamma_\omega \frac{\partial \omega}{\partial x_j} \right] \quad (3)$$

$$\frac{\partial(\rho \gamma)}{\partial t} + \frac{\partial(\rho U_j \gamma)}{\partial x_j} = P_{\gamma 1} - E_{\gamma 1} + P_{\gamma 2} - E_{\gamma 2} + \frac{\partial}{\partial x_j} \left[ \left( \mu + \frac{\mu_t}{\sigma_\gamma} \right) \frac{\partial \gamma}{\partial x_j} \right] \quad (4)$$

$$\frac{\partial(\rho \widetilde{R\theta}_{ot})}{\partial t} + \frac{\partial(\rho U_j \widetilde{R\theta}_{ot})}{\partial x_j} = P_{\theta t} + \frac{\partial}{\partial x_j} \left[ \left( \mu + \mu_t \right) \frac{\partial \widetilde{R\theta}_{ot}}{\partial x_j} \right] \quad (5)$$

where  $\widetilde{P}_k$ ,  $P_\omega$ ,  $P_{\gamma 1}$ ,  $E_{\gamma 1}$  are the production terms of the kinetic energy, specific dissipation and transition sources, respectively.  $E_k$ ,  $E_\omega$ ,  $P_{\gamma 2}$ ,  $E_{\gamma 2}$  are the destruction terms of the kinetic energy, specific dissipation and transition sources, respectively.  $D_\omega$  is the cross diffusion term and  $P_{\theta t}$  is the source term for  $\widetilde{R\theta}_{ot}$ . Also, Menter and Langtry have tested this turbulence model and shown its superiority in dealing with separated flows, and therefore this model and its original form, namely the SST  $k$ - $\omega$ , have been employed for the computations presented in this paper.

The Transition SST and the SST  $k$ - $\omega$  models are based on the Boussinesq assumption, which is built on the basis that the viscous stress and Reynolds stress have a similar effect on the mean fluid flow (Boussinesq, 1877). The limitation of this assumption on these models may be avoided by employing the Reynolds stress model and therefore an investigation was made to analyze the dynamic stall by employing this model. However, the results obtained did not achieve satisfactory convergence and in some occasions the solution diverged. This is expected due to the complexity of the dynamic stall mechanism, especially at low tip speed ratios, and also due to the mesh requirement.

The development of the dynamic stall starts near the airfoil surface and this makes employing more sophisticated turbulence models, such as the Large Eddy Simulation (LES), prohibitively computationally expensive in order to accurately analyze the fluid flow near the airfoil surface. However, the Detached Eddy Simulation (DES) may be a reasonable alternative but this model generally employs non-transitional unsteady Reynolds Averaged Navier–Stokes (URANS) models near the airfoil surface and therefore the transitional effect of the development of dynamic stall may not be resolved.

In practice, the forces exerted on the turbines airfoils, including the forces caused by the dynamic stall, produce high stresses on the turbine structure. These types of forces may be investigated by employing the Fluid–Solid Interaction (FSI) model but this aspect is not the focus of the present investigation. In the future, an investigation of this effect would be very illuminating.

The method used by the solver employed in the computation is the SIMPLE algorithm, which is a segregated pressure based solver where the pressure field is obtained by enforcing the mass conservation based on the pressure and velocity corrections (Barton, 1998; Tu et al., 2008; Versteeg and Malalasekera, 2007). All gradients are computed on the face of the cell using a least squares method.

All the simulations are run at a tip speed ratio of 1.75, which is a typical value for urban regions, and this implies that at an upwind velocity 10 m/s then the rotational speed of the turbine is 14 rad/s. Even though, the turbine could run at higher tip speed ratios, which still considered to be relatively low, a considerable time of the turbine operation could be lower than 2 where the dynamic stall presence is severe and understanding it at this level may be essential. To set similar flow conditions as in the experiment, the turbulence intensity level, the turbulent length scale and the reduced frequency are fixed in all the computations to be 0.5%, 0.028 m (0.07c) and 0.16 ( $c/d$ ), respectively. Further, the residuals are set to  $10^{-5}$  for all the variables and this is found to be sufficient for achieving convergence.

At the start of the simulations, the first-order upwind scheme, in both time and space, is applied in order to provide an initial estimate of the solution. Then, the spatial and temporal discretization is switched to second-order upwind schemes for all the computations and these are the results presented in this paper. The solution convergence is assessed based on the relative difference of the averaged torque at each time step over one revolution. At each time step, the torque produced aerodynamically by the three airfoils is calculated and the same calculation is performed for the following time steps. Then, the torque is averaged at each time step for one full rotation. When the value of the averaged torque at each time step changes by less than 2% compared to the time steps in the previous rotation, the flow is considered to have converged and the periodic torque is obtained. This could be represented mathematically by

$$\text{Convergene} = \frac{\text{Averaged torque at each time step}}{\text{Averaged torque per one revolution}} \leq 2\% \quad (6)$$

**Table 1**

Grid size and predicted power coefficient.

Grid index	Grid size (cells)	Predicted power coefficients ( $C_{p,computational}$ )	Experimental power coefficient ( $C_{p,experimental}$ )
1	495926	0.368	0.34
2	235388	0.345	
3	135506	0.295	

Four time step sizes have been employed, namely 500 (Courant  $\sim 335$ ), 1000 (Courant  $\sim 170$ ), 2500 (Courant  $\sim 65$ ) and 5000 (Courant  $\sim 32$ ) steps per one revolution. The torque obtained for the 2500 and 5000 steps are similar, however a low Courant number is desirable due to dynamic stall sensitivity and therefore 5000 steps have been applied for all the computations presented in this paper since its courant number is as low as 32. The finite volume code that is applied in all the computations is the commercial software ANSYS FLUENT, whereas GAMBIT is used to create all the meshes.

#### 4. Validation of the numerical model

One of the main challenging aspects of applying computational fluid dynamics in analyzing SB-VAWTs is to achieve a mesh independent solution that are successfully validated against the experimental data. In order to produce a mesh independent solution, two important factors have to be considered and distinguished from each other, namely mesh converged solution and iterative converged solution. When the residuals of the computed variables reach the set tolerance, the solution is considered to be iteratively converged. However, if the monitored physical variable, which is the averaged torque in this case, is not changing at each time step then the solution is considered to be a mesh converged solution. If the mesh converged solution does not change with increasing the mesh resolution, then the solution is considered to be a mesh independent solution. However, achieving a mesh independent solution in cases such as SB-VAWTs requires substantial computational time and effort. Therefore, the mesh independent solution is estimated on the basis of the Richardson Extrapolation method, which is explained thoroughly in Roache (1994, 1997, 1998) and employed for SB-VAWT mesh independency test by Almohammadi et al. (2013). Three different meshes, shown in Table 1, have been created in order to estimate the mesh independent solution for the studied SB-VAWT based on the predicted power coefficient obtained using computational fluid dynamics which is calculated from the obtained averaged torque, which is computed from the turbine blade surface by integrating the instantaneous torque over the blade surface and after that the power is computed. Time variations of torque and power are important parameters in analyzing and validating SB-VAWT CFD model. However, these data are not available for this experiment.

The formal order of accuracy of the computations is known,  $p^*=2$ , therefore extracting the order of accuracy from the three meshes is necessary in order to verify the order of accuracy. The refinement ratio ( $r$ ) between the meshes is not constant, hence  $r_{21} \neq r_{32}$  where  $r_{21} = 1.45$  and  $r_{32} = 1.32$ , and therefore the generalized theory of Richardson Extrapolation is applied. It should be noted that the grid index 1 is for the fine mesh and the grid index 3 is for the coarse mesh.

The generalized equation (Almohammadi et al., 2013) for the general Richardson Extrapolation theory is given by

$$p_{new}^* = \frac{\ln \left\{ \left( r_{12}^{p_{old}^*} - 1 \right) \left( \frac{cp_3 - cp_2}{cp_2 - cp_1} \right) + r_{12}^{p_{old}^*} \right\}}{\ln(r_{12} \ r_{32})} \quad (7)$$

which is the transcendental equation for  $p^*$  and this equation can be solved iteratively. The convergence condition is calculated using the equation:

$$R = \frac{cp_2 - cp_1}{cp_3 - cp_2} \quad (8)$$

for the results obtained by employing the transitional model, and this is found to have a value of 0.46, and therefore the convergence condition is monotonic since  $0 < R < 1$  and the generalized Richardson theory may be applied (Franke and Frank, 2008).

The extracted order of accuracy from the three meshes is 3.41 and hence it is necessary to know that the extracted order of accuracy is of the order of  $p^* + 1$  as stated by Roy (2010). Therefore, the solution is in the asymptotic range and equation:

$$Cp_{estimated} = \frac{r_{21}^{p^*} * cp_1 - cp_2}{r_{21}^{p^*} - 1} \quad (9)$$

may be employed to estimate the mesh independent solution. As a result, the estimated power coefficient is 0.388, which is slightly higher than the experimental value of about 0.34. It is expected that 2D computations will produce a power coefficient which is larger than the experimental value, and this is mainly due to the exclusion of the tip vortices and the losses due to struts on the overall performance of the turbine. It is important to note that the 2D CFD model of the SB-VAWT may substantially over predict the peak in the power coefficient of the turbine at high tip speed ratios as reviewed in Almohammadi et al. (2013). The extrapolation difference between the predicted power coefficient of the fine mesh and the estimated power coefficient using the general Richardson Extrapolation method is calculated to be about 5%, and therefore

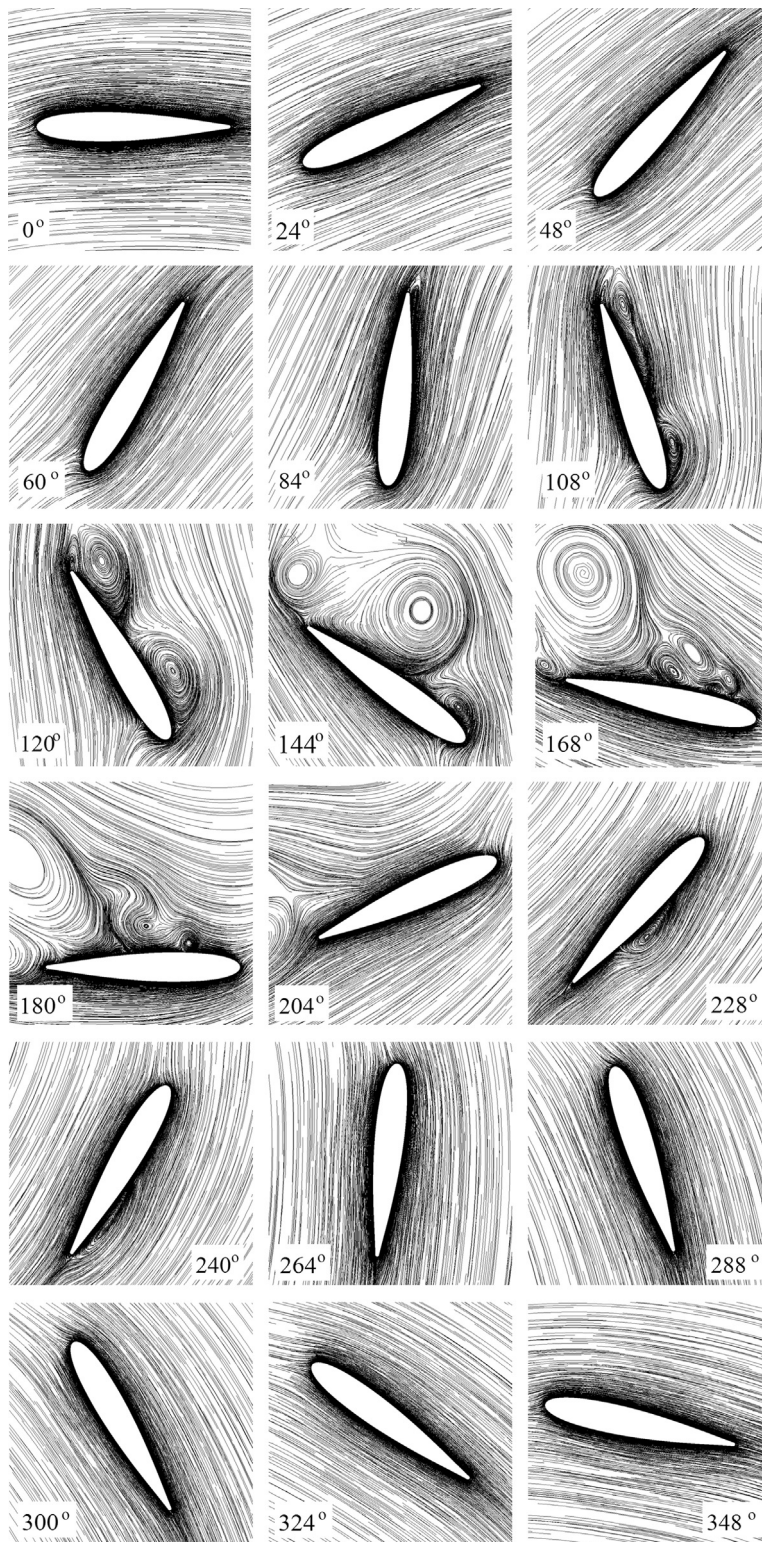


**Fig. 3.** The flow field in the vicinity of the airfoil when employing the Transition SST model during one turbine rotation.

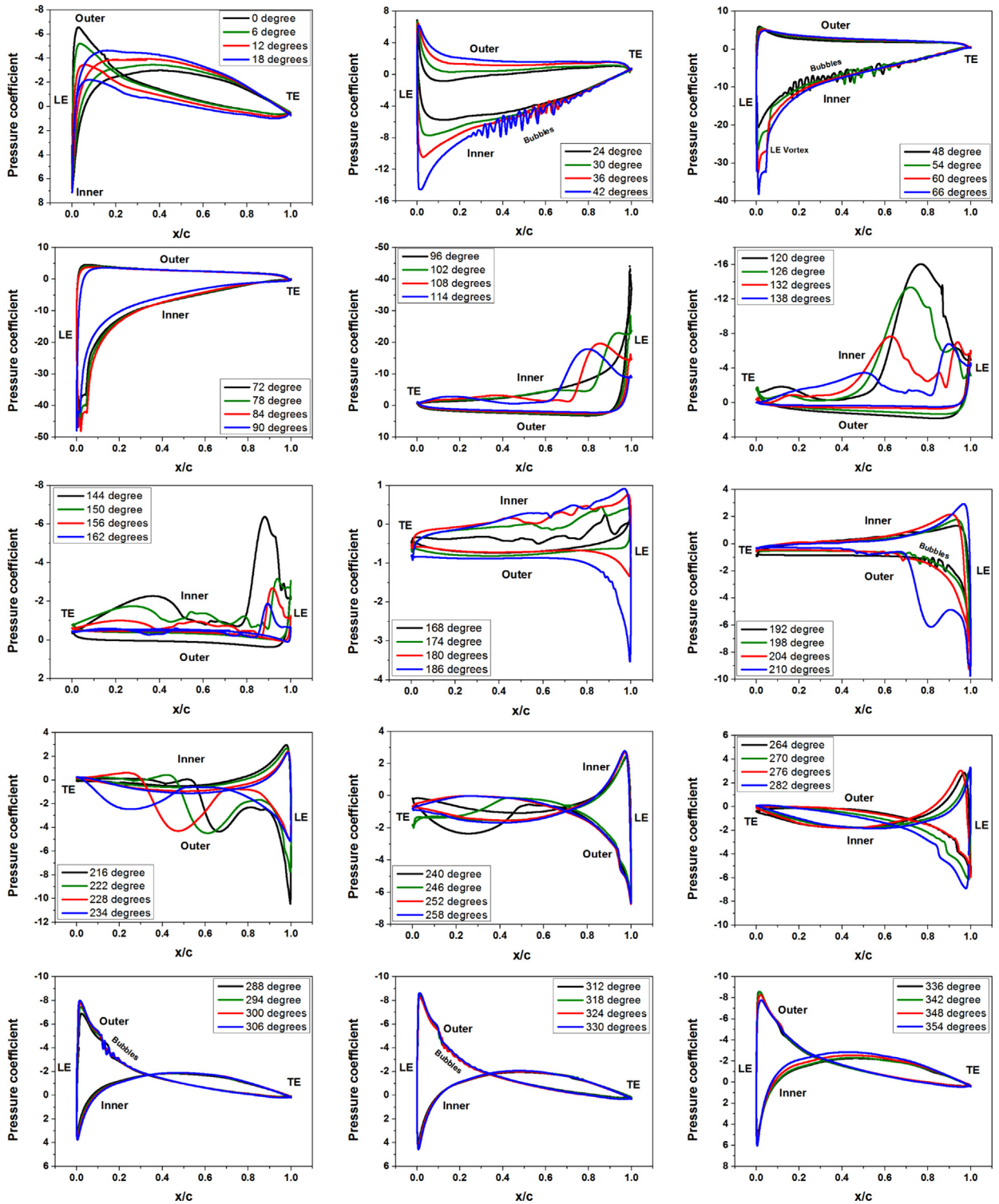


Fig. 4. Pressure coefficient distribution on the airfoil inner and outer surfaces when employing the Transition SST model during one turbine rotation (Note: for clarity, some of the pressure coefficient axes are reversed).

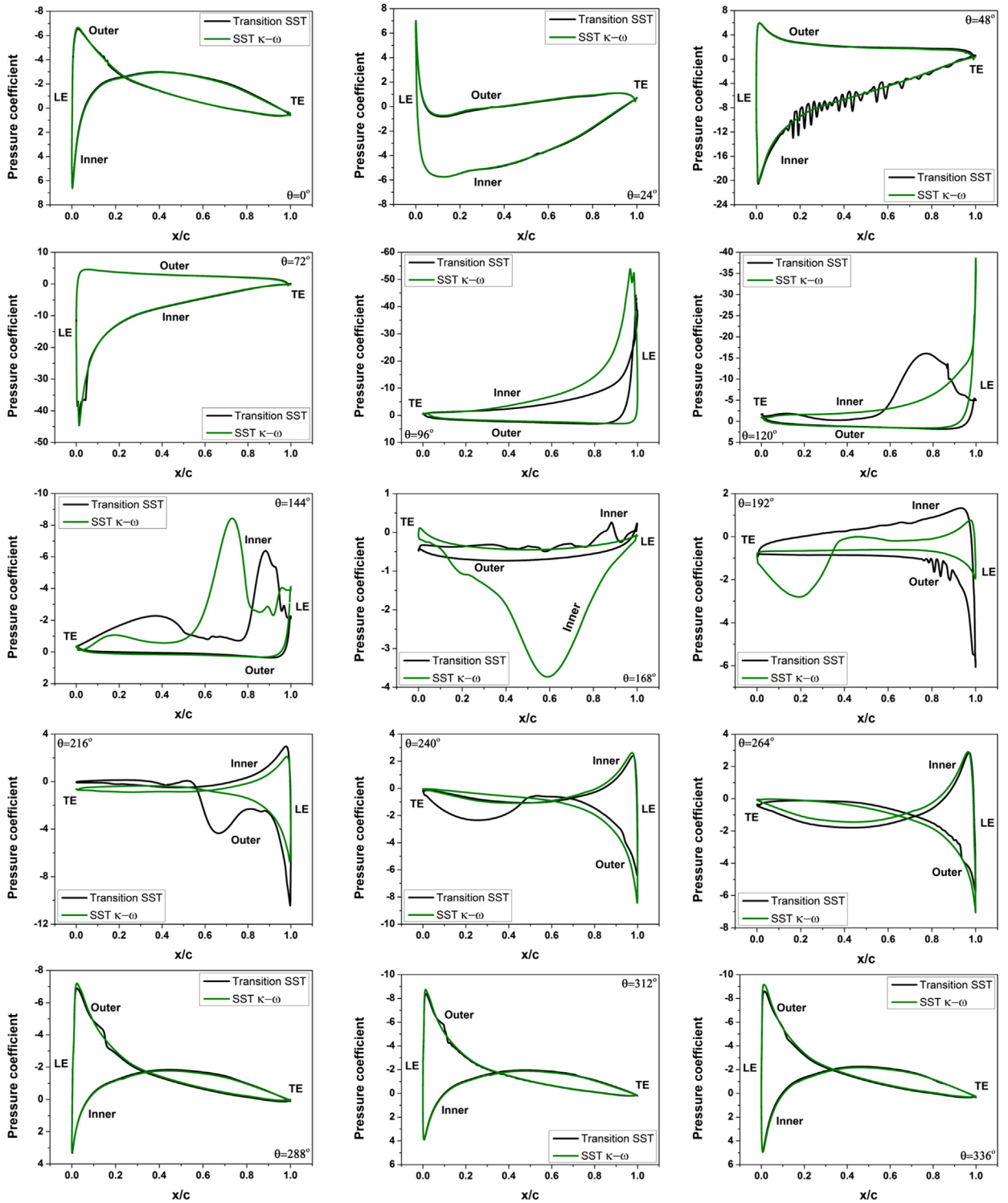


Fig. 5. The pressure distribution for the SST  $k-\omega$  and Transition SST models during one turbine rotation (Note: for clarity, some of the pressure coefficient axes are reversed).

the estimated power coefficient based on the fine mesh is considered as being a mesh independent solution and may be compared to the experimental data for validation. The power coefficient has been found to be 8.2% higher than the experimental data which is within an acceptable tolerance of the 2D computations and therefore the prediction of the fine mesh is considered to be reasonably sufficient for the purpose of the study.

## 5. Results and discussion

### 5.1. Dynamic stall

The flow development of the studied SB-VAWT when employing the transitional model at  $24^\circ$  intervals for one revolution is illustrated in Fig. 3. The development of the flow shows a small vortex being formed near the trailing edge at an angle of about  $84^\circ$ . As a result, a reversed pressure wave propagates over the inner surface of the airfoil towards the leading edge. This is followed by the formation of the leading edge vortex, as may be seen clearly at an angle of about  $108^\circ$ . The leading and trailing edge vortices grow and move towards each other and subsequently merge together at about  $144^\circ$ . This is followed by the formation of another leading and trailing edge vortices. The merged vortex continues to expand and afterwards sheds into the wake, and convects downstream of the turbine.

Up to an angle of about  $204^\circ$ , there are no clear flow disturbances or vortices on the outer surface of the airfoil. At an angle of about  $228^\circ$ , a vortex appears on the outer surface of the airfoil and moves towards the trailing edge. The general mechanism of the dynamic stall matches those found in the literature where the phenomenon has been investigated extensively in many applications, and it is well known that it is very sensitive to several parameters, such as turbine reduced frequency and the Reynolds number. Therefore, understanding the dynamic stall of vertical axis wind turbines has to be investigated using a turbine model that consists of three airfoils rotating in order to include all the factors that affect the stall phenomenon, such as the wake interactions with the airfoils. However, this requires enormous powerful computations in order to capture the dynamic stall, as shown recently in Richter et al. (2011), and for only one 2D airfoil this is computationally extremely expensive. The visualization of the flow shows a clear interaction of the leading and trailing edge vortices which certainly affects the dynamic stall and as a result the performance of the turbine.

In the downstream region of the turbine, the vortices are formed differently and there is no clear sign of the trailing edge vortex. The vortex forms near the leading edge and moves on the outer airfoil surface towards the trailing edge. However, the strength of this vortex is relatively small compared to the vortex formed upstream. In the analysis performed by Wang et al. (2012) on an oscillating airfoil, the vortices are formed only on one side of the airfoil, namely the suction side. It is important to note that Wang did not employ a symmetrical oscillation and applied a mean angle of attack of about  $10^\circ$ . However, the visualization of the flow on the three rotating airfoils of a turbine model shows that there are vortices formed on the outer surface of the airfoils on the downstream side of the turbine. The main reason for this difference is that mean angle of attack is relatively high. The angles of attack on the downstream region are relatively lower than the angles of attack on the upstream region due to the wake that affects the relative velocity and as a result the vortex formation. It is important to note that the large vortices occur due to the small changes to the fluid flow near the airfoil surface which grow and appear when their effect becomes significant. The transition may play an important role in the development of the flow near the blade which may be investigated by analyzing the pressure distribution on the airfoil as the turbine rotates.

To investigate the dynamic stall development on the airfoils, the pressure distribution on the airfoil is shown in Fig. 4 at  $6^\circ$  intervals as the airfoil rotates from an azimuthal angle  $0^\circ$ – $360^\circ$ . The trailing edge profile is curved, and this curvature induces two small local vortices behind the trailing edge due to the circulation of the flow leaving the airfoil inner and outer surfaces. As the turbine blades rotate, one of these vortices moves towards the inner side of the turbine and initiates a reversal in the pressure wave which propagates towards the leading edge. Also, at an azimuthal angle of about  $30^\circ$ , several laminar separation bubbles are formed on the inner surface of the airfoil, these bubbles move towards the leading edge of the airfoil due to the reversal in the pressure gradient and subsequently the bubbles merge to form the leading edge vortex and the bubbles disappear at about  $60^\circ$ . The main reason for the bubble formation is the presence of the adverse pressure gradient. However, another possible reason is the effect of the Reynolds number, which affects the pressure distribution on the airfoil, airfoil shape, and flow conditions (Tani, 1964). Therefore, it appears that the leading edge vortex in the vertical

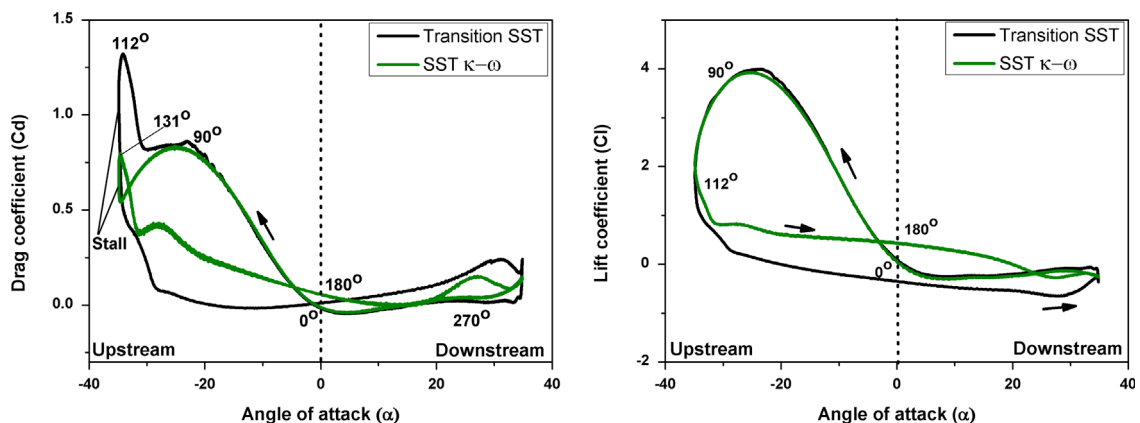


Fig. 6. Lift and drag versus the angle of attack for the SST  $k-\omega$  and the Transition SST models during one turbine rotation.

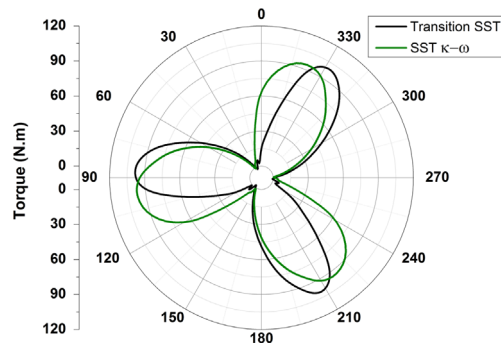


Fig. 7. Torque roses produced by SB-VAWT for the SST  $k-\omega$  and the Transition SST models for one turbine rotation.

axis wind turbines is mainly initiated by the laminar separation bubbles which are formed due to the laminar-turbulent transition on the inner surface of the airfoil upstream of the turbine. The movement of the leading and trailing edge vortices are clearly seen in the pressure coefficient distribution between  $102^\circ$  and  $144^\circ$  in Fig. 4. The reattachment of the flow on the inner surface of the airfoil is obtained at an azimuthal angle of about  $192^\circ$ , at which small laminar separation bubbles are formed on the outer surface of the airfoil. In contrast to the bubbles formed upstream of the turbine, these bubbles are relatively small and there is no sign of the trailing edge vortex moving towards the leading edge. However, it is important to note that these bubbles grow and move towards the trailing edge of the airfoil where they shed into the wake. As the airfoil approaches the starting point of the rotation, namely the azimuthal angle of zero degrees, the laminar separation bubbles become smaller and eventually vanish and the pressure coefficient distribution becomes uniform over both sides of the airfoil. The general mechanism of initiating the reversal in the pressure wave over the airfoil, which later moves the laminar separation bubbles towards the leading edge found in this study agrees to the findings of several researchers in different fields (Alam and Sandham, 2000; Jones, 1933, 1934; Mayda and Van Dam, 2002). The flow characteristic of SB-VAWT shows that it combines two types of stall, namely the trailing edge vortex moving towards the leading edge and the leading edge vortex moving towards the trailing edge. The laminar separation bubbles add complexity to the modeling of the flow around the airfoil and thus reduce the performance of the wind turbine. These bubbles are not always present and only exist in certain flow conditions. If the modeling of the SB-VAWT includes improving the design, then controlling these bubbles is vital in enhancing the overall performance of the turbine.

## 5.2. Transition and laminar separation bubbles

The presence of the laminar separation bubbles is not desirable due to their effect on the turbine performance. As a fundamental research topic, the laminar separation bubbles have been extensively studied for many different applications (Jones, 1933, 1934; Mehta and Lavan, 1975; Rist and Maucher, 2002; Rist et al., 1996; Tani, 1964; Yang et al., 2008). The formation of the bubbles is mainly caused by the laminar-turbulent transition as the boundary layer separates due to the transition, and reattaches due to the turbulence. This process is known to be the result of the change in the local Reynolds number and/or the increase in the angle of attack. It is important to estimate the effect of the bubbles on the turbine performance, especially if we are to redesign or optimize the SB-VAWT. This is very important since the change in the airfoil shape could cause or reduce the bubbles, and as a result the turbine performance would be either over, or under, estimated. The effect of the laminar separation bubble could be studied by comparing the turbine performance by applying the results obtained against the non-transitional model, namely the SST  $k-\omega$  model. It is clear from the pressure distribution on the airfoil in Fig. 5 that the bubbles are not predicted when applying the non-transitional model, which is clear due to the transitional state of the bubbles. The power coefficient produced when employing the transitional model is predicted to be 0.368, whereas it is 0.441 if the transition model is not applied. It is important to highlight that all the parameters are fixed in both cases apart from the turbulence model, and this yielded a difference in the power prediction of about 20% in the turbine performance. Therefore, if the transitional model is not employed, any enhancement in the predicted power coefficient due to geometrical changes in the turbine, or its flow conditions, could be caused by suppressing the effect of the laminar separation bubbles. It is also important to highlight that the leading edge bubble is predicted only by the transitional model, which may be observed at an azimuthal angle of about  $72^\circ$ . Between the azimuthal angles  $72^\circ$  and  $264^\circ$ , the pressure distribution on the airfoil surface is not similar for the SST  $k-\omega$  and the Transition SST models, and this suggests the strong effect of the transition modeling on the SB-VAWT in the dynamic stall conditions. Between angles of  $264^\circ$  and  $0^\circ$ , the transitional effect is gradually reduced, and as a result the pressure distribution becomes similar for both turbulence models. Therefore, the transitional modeling is substantially more important in the design and optimization process of the SB-VAWTs since the power coefficient may be over, or under, predicted by the laminar-turbulent transition of the air flow if a transitional model is not employed.

Fig. 6 shows the lift and drag at different angles of attack for one revolution. The angle of attack varies between about  $\pm 35^\circ$  based on the upwind velocity. The lift and drag are defined as the force perpendicular and parallel, respectively, to the

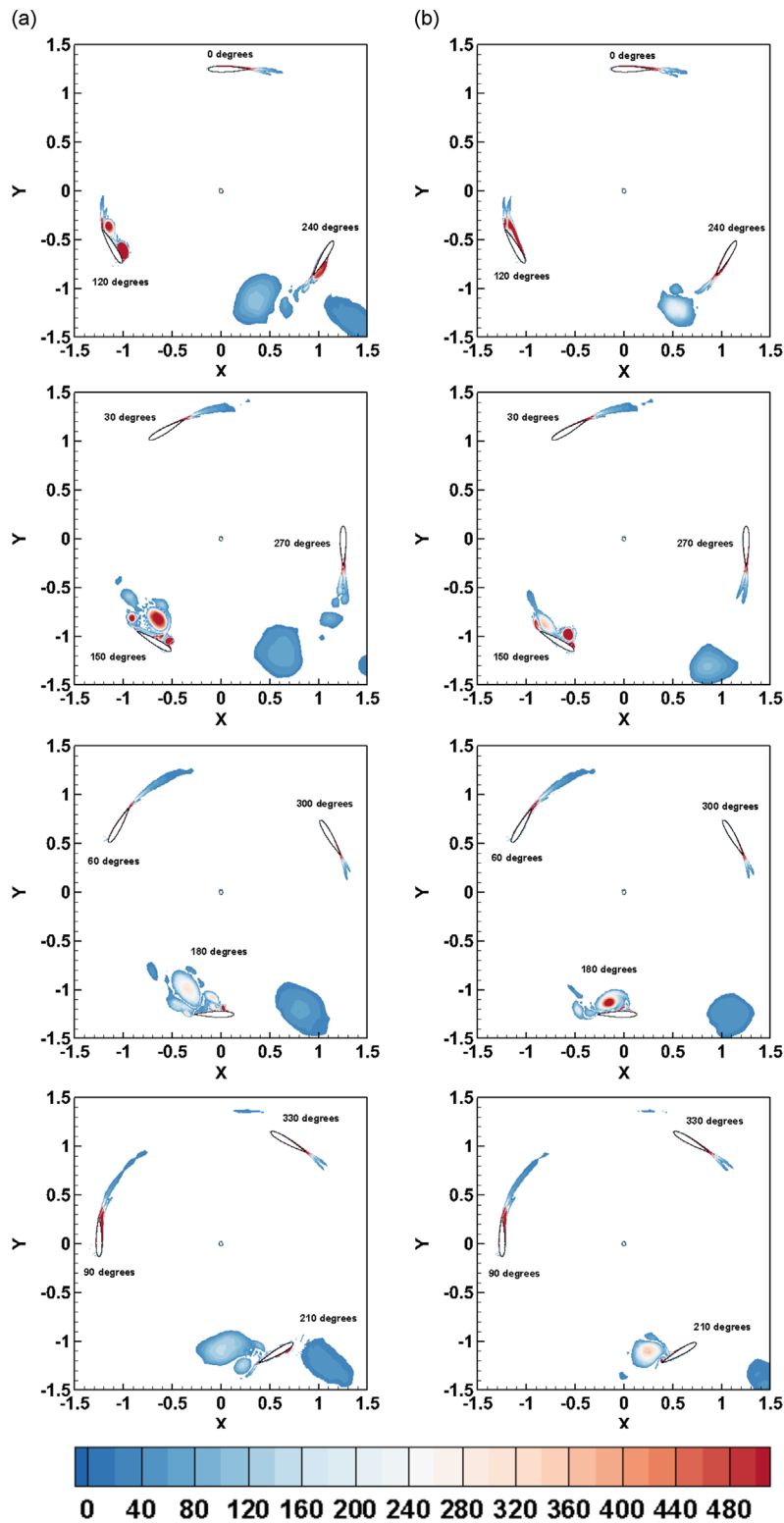


Fig. 8. Magnitude of the flow field vorticity produced by SB-VAWT for (a) the Transition SST and (b) the SST  $k-\omega$  models at TSR 1.75.

flow seen by the airfoil. It is clear that lift coefficient for the Transition SST and SST  $k-\omega$  is significantly different when the airfoil is in the stall condition, particularly after the stall occurrence at an angle of attack of about  $-35^\circ$  up to about  $35^\circ$ . This suggests a strong sensitivity of the transitional modeling on the dynamic stall and the flow recovery after the dynamic stall

occurrence. The Transitions SST model has predicted the dynamic stall earlier than the SST  $k-\omega$  by an azimuthal angle of about  $19^\circ$  as it is seen in the drag coefficient. After the stall occurrence, the flow recovery is significantly different and this is clear in both the lift and drag coefficient where the lift and drag are over predicted by SST  $k-\omega$  model in the upstream side and under predicted in the downstream side compared to the Transition SST model prediction of the lift and drag. The prediction of the two models remained significantly different for an azimuthal angle about  $160^\circ$ . The shedding of the vortices from the airfoil surface and convection downstream of the turbine is clearly a source of difference in the lift and drag predictions, and accounting for transition seems to play a significant role on the formation of these vortices. It is important to highlight that the  $k-\omega$  models do not accurately predict the recovery of air flow in some applications (Versteeg and Malalasekera, 2007). Further research is required to investigate the flow recovery after the airfoil stall occurs.

The torque roses of the turbine for both models, namely the SST  $k-\omega$  and the Transition SST models, are compared in Fig. 7 (Castelli and Benini, 2012). The predicted torque of the turbine peaks at an azimuthal angle of about  $86^\circ$ ,  $206^\circ$ , and  $326^\circ$  when employing the Transition SST model. On the other hand, the predicted torque of the turbine peaks at an azimuthal angle of about  $97^\circ$ ,  $217^\circ$ , and  $337^\circ$  when employing the SST  $k-\omega$  model. Thus the azimuthal location of the torque peak of the turbine is delayed by about  $11^\circ$  when employing non-transitional model. The main reason for this is that the effect of the flow transition on the airfoil boundary layer is not captured by the non-transitional models. The small laminar separation bubbles, the vortex formation and the dynamic stall process start in the boundary layer where the air flow transition takes place. Therefore, the non-transitional model does not account for these small events which significantly affect the air flow development near the airfoil and the overall performance of the turbine.

The effect of the delay in prediction of the dynamic stall due to employing the non-transitional model may be seen in Fig. 8 where the magnitude of the flow field vorticity is presented. It may be observed that the magnitude of the flow field vorticity near the airfoil is similar for azimuthal angles  $0-90^\circ$ . However, between angles  $90^\circ$  and  $270^\circ$  the airfoil is under the effect of the dynamic stall and therefore the effect of delayed prediction of the dynamic stall when employing the non-transitional model may be clearly visualized in the vicinity of the airfoil. As the airfoil approaches the azimuthal angle  $270^\circ$ , the severity of the dynamic stall gradually decreases and as a result no significant differences in the magnitude of the flow field vorticity may be observed. This confirms the significance of the fluid flow transition within the airfoil boundary layer in SB-VAWTs in the development of the dynamic stall. However, it should be noted that the power coefficient of the investigated turbine peaks around the investigated tip speed ratio, namely 1.75, and this makes the wake interaction with downstream blade minimal and therefore the wake interaction with the downstream blade is not significant.

## 6. Conclusions

In this paper, the 2D Navier–Stokes equations have been employed to investigate the dynamic stall process. The principle of the General Richardson Extrapolation technique has been applied in order to estimate the mesh independent solution of the numerical computations obtained from three different meshes. Two turbulence models have been employed for all the computations presented in this paper, namely the SST  $k-\omega$  and the Transition SST model. It has been found that dynamic stall in SB-VAWTs combine two processes. The first is the formation of the vortex near the trailing edge of the airfoil which propagates towards the leading edge, whereas the second is the formation of the leading edge vortex which moves towards the trailing edge. At some stage, the two vortices merge together to form one larger vortex which consequently sheds into the wake.

The transitional effect is found to be vital in predicting the dynamic stall and we have found that the stall is predicted earlier when the transitional model is applied than for the SST  $k-\omega$  model. This has been observed on the shift of the torque roses by about  $11^\circ$  obtained numerically for the turbine investigated and also visualized using the magnitude of the flow field vorticity. The small laminar separation bubbles could be predicted only when applying the transitional model. If the transitional model is not applied in the design or optimization processes, any change in the predicted performance could be due to the separation bubbles and the flow transition which could create a difference in the power predictions by up to 20%.

Controlling the laminar separation bubbles produced by the SB-VAWTs could be a method to improve the overall performance of the turbine and a future research area that needs to be further investigated. Further studies should be directed towards the mesh independency tests due to the high sensitivity of the dynamic stall phenomenon.

## Acknowledgments

Khaled M. Almohammadi would like to express his gratitude to Taibah University, Kingdom of Saudi Arabia for supporting him to perform his Ph.D. study at the University of Leeds.

## References

- Acheson, D., 1990. *Elementary Fluid Dynamics*. Oxford University Press, USA, New York.
- Alam, M., Sandham, N., 2000. Direct numerical simulation of 'short' laminar separation bubbles with turbulent reattachment. *Journal of Fluid Mechanics* 410, 1–28.
- Almohammadi, K., Ingham, D., Ma, L., Pourkashan, M., 2013. Computational fluid dynamics (CFD) mesh independency techniques for a straight blade vertical axis wind turbine. *Energy* 58, 483–493.

- Apsley, D., Chen, W.-L., Leschziner, M., Lien, F.-S., 1997. Nonlinear eddy viscosity modelling of separated flows. *IAHR Journal of Hydraulic Research* 35, 723–748.
- Balduzzi, F., Bianchini, A., Carnevale, E.A., Ferrari, L., Magnani, S., 2012. Feasibility analysis of a Darrieus vertical-axis wind turbine installation in the rooftop of a building. *Applied Energy* 97, 921–929.
- Baldwin, B., Lomax, H., 1978. Thin Layer Approximation and Algebraic Model for Separated Turbulent Flows. AIAA Paper, 78-257.
- Barton, I., 1998. Comparison of SIMPLE and PISO type algorithms for transient flows. *International Journal for Numerical Methods in Fluids* 26, 459–483.
- Boussinesq, J., 1877. Théorie de l'écoulement tourbillant. *Mémoires Présentés par Divers Savans à l'Académie Royale des Sciences de l'Institut de France* 23, 46–50.
- Bravo, R., Tullis, S., Ziada, S., 2007. Performance testing of a small vertical-axis wind turbine. In: *Proceedings of the 21st Canadian Congress of Applied Mechanics*. Toronto, Ontario, Canada, pp. 470–471.
- Cardona, J., 1984. Flow curvature and dynamic stall simulated with an aerodynamic free-vortex model for VAWT (vertical axis wind turbine). *Wind Engineering* 8, 135–143.
- Carr, L.W., 1988. Progress in analysis and prediction of dynamic stall. *Journal of Aircraft* 25, 6–17.
- Carta, F.O., 1979. A Comparison of the Pitching and Plunging Response of an Oscillating Airfoil. National Aeronautics and Space Administration, Scientific and Technical Information Branch, Washington, DC, USA1–164.
- Castelli, M.R., Benini, E., 2012. Effect of blade inclination angle on a Darrieus wind turbine. *Journal of Turbomachinery* 134, 1–10.
- Castelli, M.R., Englaro, A., Benini, E., 2011. The Darrieus wind turbine: proposal for a new performance prediction model based on CFD. *Energy* 36, 4919–4934.
- Eckhardt, B., Schneider, T., Hof, B., Westerweel, J., 2007. Turbulence transition in pipe flow. *Fluid Mechanics* 39, 447–468.
- Ericsson, L.E., Reding, J.P., 1983. The difference between the effects of pitch and plunge on dynamic airfoil stall. In: *Proceedings of the 9th European Rotorcraft Forum*. Stresa, Italy, pp. 1–8.
- Favier, D., Agnes, A., Barbi, C., Maresca, C., 1988. Combined translation/pitch motion – a new airfoil dynamic stall simulation. *Journal of Aircraft* 25, 805–814.
- Ferreira, C.S., Bijl, H., Van Bussel, G., Van Kuik, G., 2007. Simulating dynamic stall in a 2D VAWT: modeling strategy, verification and validation with particle image velocimetry data. *Journal of Physics: Conference Series*. IOP Publishing, 012023.
- Ferreira, C.S., Kuik, G.V., Bussel, G.V., Scarano, F., 2009. Visualization by PIV of dynamic stall on a vertical axis wind turbine. *Experiments in Fluids* 46, 97–108.
- Franke, J., Frank, W., 2008. Application of generalized Richardson extrapolation to the computation of the flow across an asymmetric street intersection. *Journal of Wind Engineering and Industrial Aerodynamics* 96, 1616–1628.
- Fraunie, P., Beguier, C., Paraschivoiu, I., Brochier, G., 1986. Water channel experiments of dynamic stall on darrieus wind turbine blades. *Journal of Propulsion and Power* 2, 445–449.
- Fujisawa, N., Shibuya, S., 2001. Observations of dynamic stall on darrieus wind turbine blades. *Journal of Wind Engineering & Industrial Aerodynamics* 89, 201–214.
- Gharali, K., Johnson, D.A., 2012. Numerical modeling of an S809 airfoil under dynamic stall, erosion and high reduced frequencies. *Applied Energy* 93, 45–52.
- Gupta, R., Biswas, A., 2010. Computational fluid dynamics analysis of a twisted three-bladed H-Darrieus rotor. *Journal of Renewable and Sustainable Energy* 2, 043111–043126.
- Ham, N.D., 1968. Aerodynamic loading on a two-dimensional airfoil during dynamic stall. *AIAA Journal* 6, 1927–1934.
- Hwang, I.S., Lee, Y.H., Kim, S.J., 2009. Optimization of cycloidal water turbine and the performance improvement by individual blade control. *Applied Energy* 86, 1532–1540.
- Ince, N., Launder, B., 1995. Three-dimensional and heat-loss effects on turbulent flow in a nominally two-dimensional cavity. *International Journal of Heat and Fluid Flow* 16, 171–177.
- Islam, M., Amin, M.R., Carriveau, R., Fartaj, A., 2009. Investigation of low reynolds number airfoils for fixed-pitch straight-bladed VAWT. In: *Proceedings of the 47th AIAA Aerospace Sciences Meeting including the New Horizons Forum and Aerospace Exposition*. American Institute for Aeronautics and Astronautics, Orlando, Florida, USA.
- Islam, M., Ting, D., Fartaj, A., 2008. Aerodynamic models for Darrieus-type straight-bladed vertical axis wind turbines. *Renewable and Sustainable Energy Reviews* 12, 1087–1109.
- Jackson, D., Launder, B., 2007. Osborne Reynolds and the publication of his papers on turbulent flow. *Fluid Mechanics* 39, 19–35.
- Jones, B.M., 1933. An Experimental Study of the Stalling of Wings British ARC. Aeronautical Research Committee Reports and Memoranda, London.
- Jones, B.M., 1934. Stalling. *Journal of Royal Aeronautical Society* 38, 753–770.
- Kato, M., Launder, B., 1993. Three-dimensional modelling and heat-loss effects on turbulent flow in a nominally two-dimensional cavity. *International Journal of Heat and Fluid Flow* 16, 171–177.
- Kooiman, S., Tullis, S., 2010. Response of a vertical axis wind turbine to time varying wind conditions found within the urban environment. *Wind Engineering* 34, 389–401.
- Laneville, A., Vittecoq, P., 1986. Dynamic stall: the case of the vertical axis wind turbine. *Journal of Solar Energy Engineering* 108, 140.
- Langtry, R., Menter, F., Likki, S., Suzen, Y., Huang, P., Völker, S., 2006. A correlation-based transition model using local variables—Part II: test cases and industrial applications. *Journal of Turbomachinery* 128, 423.
- Leishman, J., 1990. Dynamic stall experiments on the NACA 23012 aerofoil. *Experiments in Fluids* 9, 49–58.
- Leishman, J.G., 2006. *Principles of Helicopter Aerodynamics*, 2nd ed. Cambridge University Press, Cambridge, New York, USA.
- Mayda, E.A., Van Dam, C.P., 2002. Bubble-induced unsteadiness on a wind turbine airfoil. *Journal of Solar Energy Engineering* 124, 335–345.
- McAlister, K., 1982. An Experimental Study of Dynamic Stall on Advanced Airfoil Sections. Vol. 2. Pressure and Force Data. DTIC Document.
- McCroskey, W., Carr, L., McAlister, K., 1975a. Dynamic stall experiments on oscillating airfoils. *AIAA Journal* 14, 57–63.
- McCroskey, W.J., Carr, L.W., McAlister, K.W., 1975b. Dynamic stall experiments on oscillating airfoils. *AIAA Journal* 14, 57–63.
- McCroskey, W.J., McAlister, K.W., Carr, L.W., Pucci, S.L., 1982. An Experimental Study of Dynamic Stall on Advanced Airfoil Sections. Volume 1: Summary of the experiment. National Aeronautics and Space Administration, Technical Memorandum, Langley Station, USA, p. 679.
- McLaren, K.W., 2011. A numerical and Experimental Study of Unsteady Loading of High Solidity Vertical Axis Wind Turbines, Mechanical Engineering. McMaster University, McMaster1–251.
- Mehta, U.B., Lavan, Z., 1975. Starting vortex, separation bubbles and stall – a numerical study of laminar unsteady flow around an airfoil. *Journal of Fluid Mechanics* 67, 227–256.
- Menter, F.R., 2009. Review of the shear-stress transport turbulence model experience from an industrial perspective. *International Journal of Computational Fluid Dynamics* 23, 305–316.
- Menter, F.R., Kuntz, M., Langtry, R.B., 2003. Ten years of industrial experience with the SST turbulence model. In: *Proceedings of the 4th International Symposium on Turbulence, Heat and Mass Transfer*, Antalya, Turkey, pp. 625–632.
- Menter, F.R., Langtry, R.B., Likki, S.R., Suzen, Y.B., Huang, P.G., Völker, S., 2006. A correlation-based transition model using local variables—Part I: model formulation. *Journal of Turbomachinery* 128, 413–422.
- Mulleners, K., Raffel, M., 2011. The onset of dynamic stall revisited. *Experiments in Fluids*, 1–15.
- Paraschivoiu, I., 1988. Double-multiple streamtube model for studying vertical-axis wind turbines. *Journal of Propulsion and Power* 4, 370–377.
- Paraschivoiu, I., 2002. *Wind Turbine Design: With Emphasis on Darrieus Concept*. Polytechnic International Press, Montréal, Canada.
- Paraschivoiu, I., Delclaux, F., 1983. Double multiple streamtube model with recent improvements. *Journal of Energy* 7, 250–255.

- Reynolds, O., 1895. On the dynamical theory of turbulent incompressible viscous fluids and the determination of the criterion. *Philosophical Transactions of the Royal Society A* 186, 123–161.
- Richter, K., Le Pape, A., Knopp, T., Costes, M., Gleize, V., Gardner, A., 2011. Improved two-dimensional dynamic stall prediction with structured and hybrid numerical methods. *Journal of the American Helicopter Society* 56, 1–12.
- Rist, U., Maucher, U., 2002. Investigations of time-growing instabilities in laminar separation bubbles. *European Journal of Mechanics – B/Fluids* 21, 495–509.
- Rist, U., Maucher, U., Wagner, S., 1996. Direct numerical simulation of some fundamental problems related to transition in laminar separation bubbles. *Computational Methods in Applied Sciences* 96, 319–325.
- Roache, P.J., 1994. Perspective: a method for uniform reporting of grid refinement studies. *Journal of Fluids Engineering* 116, 405–413.
- Roache, P.J., 1997. Quantification of uncertainty in computational fluid dynamics. *Annual Review of Fluid Mechanics* 29, 123–160.
- Roache, P.J., 1998. *Fundamentals of Computational Fluid Dynamics*. Hermosa Publishers, New Mexico, USA.
- Roy, C.J., 2010. Review of discretization error estimators in scientific computing. In: *Proceedings of the 48th AIAA Aerospace Sciences Meeting Including the New Horizons Forum and Aerospace Exposition, Orlando, Florida, USA*, pp. 126–155.
- Sharpe, D.J., 1977. *A Theoretical and Experimental Study of the Darrieus Vertical Axis Wind Turbine*. Polytechnic School of Mechanical, Aeronautical and Production Engineering, Kingston, UK.
- Strickland, J., Webster, B., Nguyen, T., 1980. *Vortex Model of the Darrieus Turbine: An Analytical and Experimental Study*. SAND-79-7058. Texas Tech University, Lubbock, USA.
- Tani, I., 1964. Low-speed flows involving bubble separations. *Progress in Aerospace Sciences* 5, 70–104.
- Tsang, K.K.Y., So, R.M.C., Leung, R.C.K., Wang, X.Q., 2008. Dynamic stall behavior from unsteady force measurements. *Journal of Fluids and Structures* 24, 129–150.
- Tu, J., Yeoh, G.H., Liu, C., 2008. *Computational Fluid Dynamics: A Practical Approach*, 1st ed. Butterworth-Heinemann, Boston, USA.
- Versteeg, H., Malalasekera, W., 2007. *An Introduction to Computational Fluid Dynamics: The Finite Volume Method*. Prentice Hall.
- Wang, S., Ingham, D.B., Ma, L., Pourkashanian, M., Tao, Z., 2010a. Numerical investigations on dynamic stall of low Reynolds number flow around oscillating airfoils. *Computers & Fluids* 39, 1529–1541.
- Wang, S., Ingham, D.B., Ma, L., Pourkashanian, M., Tao, Z., 2012. Turbulence modeling of deep dynamic stall at relatively low Reynolds number. *Journal of Fluids and Structures* 33, 191–209.
- Wang, S., Ma, L., Ingham, D.B., Pourkashanian, M., Tao, Z., 2010b. Turbulence modelling of deep dynamic stall at low Reynolds number. *Lecture Notes in Engineering and Computer Science* 2184, 1350–1355.
- Yang, Z., Igarashi, H., Martin, M., Hu, H., 2008. An experimental investigation on aerodynamic hysteresis of a low-Reynolds number airfoil. In: *Proceedings of the 46th AIAA Aerospace Sciences Meeting and Exhibit*. American Institute of Aeronautics and Astronautics, Reno, Nevada, USA.